My Thesis Title

Philip Gemmell
Oriel College

Computational Biology Research Group
Computing Laboratory
University of Oxford

Define Term

This thesis is submitted to the Computing Laboratory, University of Oxford, for the degree of Doctor of Philosophy. This thesis is entirely my own work, and, except where otherwise indicated, describes my own research.

Philip Gemmell
Oriel College

Doctor of Philosophy
Define Term

My Thesis Title

Abstract

This thesis describes stuff aplenty.

Contents

List of Figures

List of Tables

Acknowledgements

This thesis is the culmination of many year's work and would not have been possible without the help and support of many people.

AP	Action Potential
$\mathrm{AP}_{\mathrm{RMS}}$	Root mean square difference between 'test' and 'training' data for V_m data
APD_x	Action potential duration to x% repolarisation
$[\mathrm{Ca}^{2+}]_{\mathrm{i}}$	Free cytosolic Ca^{2+} concentration
g_X	Maximum conductance for current X
$I_{\mathrm{Ca,L}}$	L-type Ca^{2+} current
I_{K1}	Inward rectifying K^{+} current
I_{Kr}	Rapidly delayed rectifier K^{+} current
I_{Ks}	Slowly delayed rectifier K^{+} current
I_{Na}	Na^{+} current
I_{NaCa}	Na^{+}-Ca^{2+} exchanger current
I_{NaK}	Na^{+}-K^{+} pump current
I_{stim}	Stimulus current
I_{to}	K^{+} transient outward current
$I_{\mathrm{to,f}}$	Fast K^{+} transient outward current
$I_{\mathrm{to,s}}$	Slow K^{+} transient outward current
V_m	Membrane potential
$\Delta[\mathrm{Ca}^{2+}]_{\mathrm{i}}$	Difference between systolic $[\mathrm{Ca}^{2+}]_{\mathrm{i}}$ and diastolic $[\mathrm{Ca}^{2+}]_{\mathrm{i}}$

1 Introduction

This will be the introduction.

2 Literature Review

There are more things in heaven and earth, Horatio,
Than are dreamt of in your philosophy. (*Hamlet*, Act 1, Scene 5)

In this section, the relevant background information is given. This starts with a brief outline of the function and structure of the heart, ranging from the high order organisation of the heart into functional compartments, down to the cellular level. Further details are then given on the physiological aspects of some of the subcellular components of cardiac tissue. The evolution of computational models to describe the electrical activity of the heart is charted briefly, with special attention given to models specifically used in this thesis. Variation is then described, both in experimental and physiological measurements, and how this variation has been addressed in computational models. Then the pathological condition of ischæmia will be described, and the computational efforts to model this outlined.

2.1 Cardiac Physiology

At the most general level, the heart serves as a pump to transport blood around the body to deliver nutrients and remove waste products. It does this by rhythmic, organised contraction—the rate of this contraction varies depending on species, age, condition of the heart and the activity being undertaken by the organism.

2.1.1 Structure of the Mammalian Heart

Fig. 2.1 shows the anatomical structure of the mammalian heart—while the size obviously varies widely between mammals, the overall architecture remains constant. It is split into two halves, left and right, by a muscular wall called the *septum*, and then further subdivided into two chambers, the larger, lower chamber being a *ventricle*, and the smaller, upper chamber called an *atrium*.

The passage of blood through the heart follows thus: firstly, deoxygenated blood from the body enters the heart via the superior and inferior/posterior *vena cava*, with superior and inferior representing whether the blood comes from the upper or lower half of the body

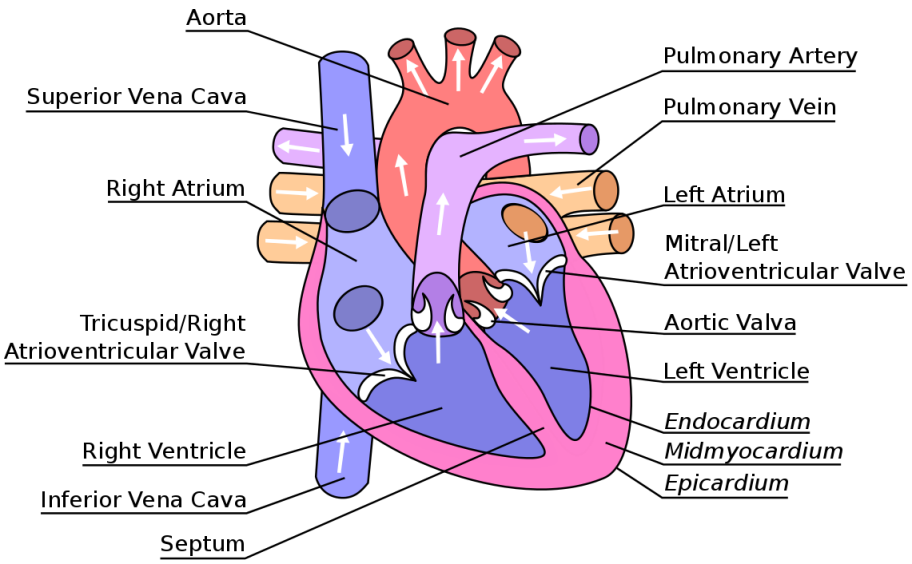

Figure 2.1: *Diagram of the longitudinal cross-section of a mammalian heart. The direction of blood flow is shown by white arrows, and all major structural components are labelled.*

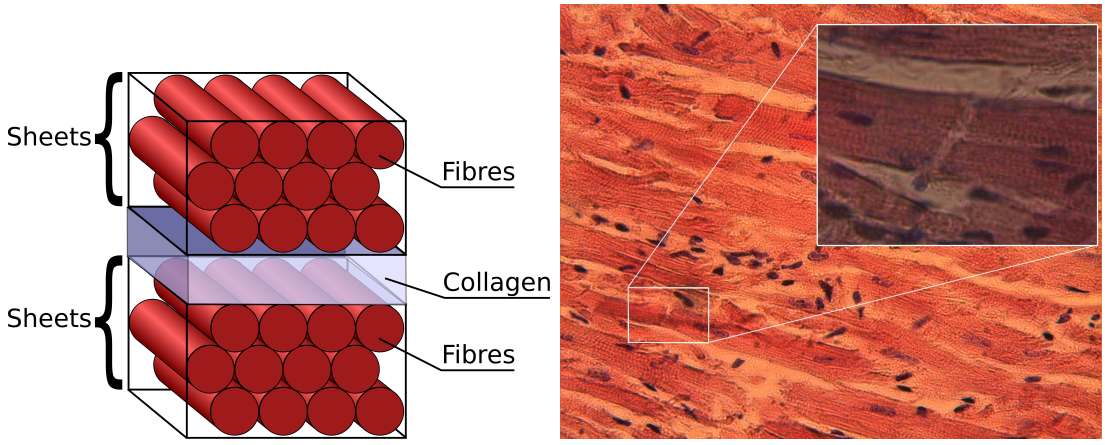

(a) *Schematic* **(b)** *Image*

Figure 2.2: *(2.2a) Schematic of the structure of myocardial sheets and fibres. (2.2b) Image of cardiomyocytes demonstrating the interconnected nature of the individual myocytes into fibres.*

respectively. Via this channel, it enters the *right atrium*. Passing through the *tricuspid valve* (also known as the right atrioventricular valve), the blood enters the *right ventricle*, where it is then pumped via the *pulmonary artery* to the lungs, where it is oxygenated. The blood returns to the heart via the *pulmonary vein*, entering the *left atrium*, before moving through the *mitral valve* (also known as the left atrioventricular valve) into the *left ventricle*. The blood is then pumped via the *aorta* to the rest of the body. The valves in the heart serve to ensure the flow of blood is always in the correct direction.

The walls of the heart are mostly composed of muscular tissue known as *myocardium*. The thickness of the myocardium is not constant throughout the heart, being thickest in the left ventricle, which requires the greatest force of contraction to pump the blood from the heart to the rest of the body. The myocardium can be split into three different regimes, as labelled in italics in Fig. 2.1: the *epicardium* is the outermost layer of the myocardium, the *midmyocardium* is the middle layer, and the *endocardium* is the innermost layer. The cells composing these different layers possess different electrophysiological properties; the differences, and the consequences, will be expanded upon in §2.1.2.

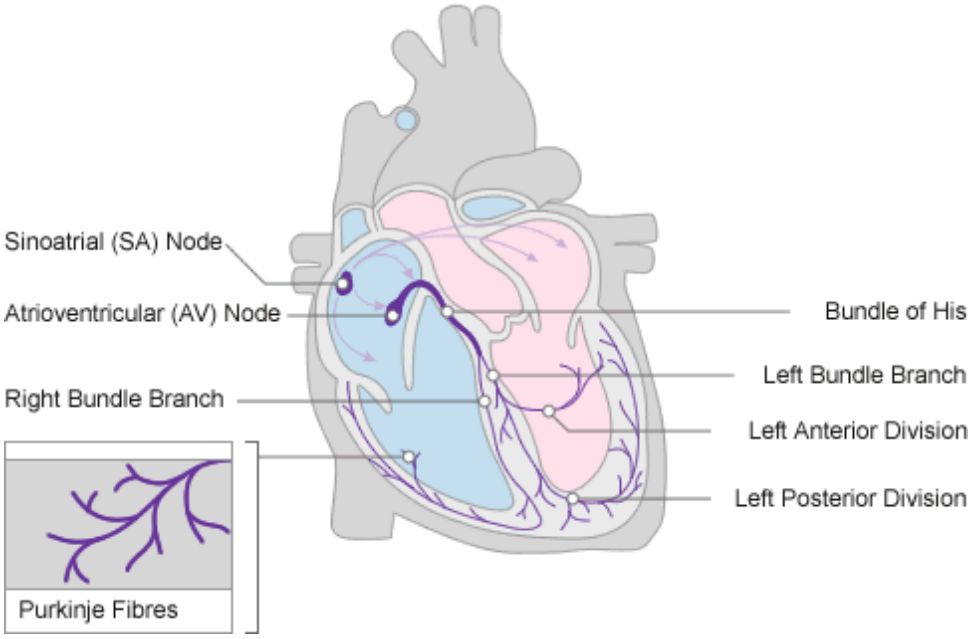

Figure 2.3: *Schematic outline of the sequence of electrical activation in the mammalian heart. Image originally downloaded from www.nottingham.ac.uk on 10th December 2012.*

The structure within the myocardium is shown in Fig. 2.2a: it is composed of a series of sheets of tissue separated by collagen. The myocytes themselves lie longitudinally in these sheets to form fibres, with myocytes in the fibre direction connected to each other by intercalated discs (as opposed to skeletal muscle, which is composed of multinucleated fibres); this structure is seen in Fig. 2.2b. One attribute of these discs is the presence of *gap junctions*, which serve to electrically couple the myocytes by allowing ion flow between the two neighbouring myocytes in the fibre direction. This arrangement of the myocytes into electrically coupled fibres allows for coordinated contraction, and the fibrous structure allows the heart to twist as it contracts, leading to a more efficient pumping mechanism.

The conduction pattern of the heart is key to the effective pumping mechanism—by controlling the sequence of electrical events in the heart, the sequence of conduction is similarly controlled. An outline of the conduction pattern of the heart is shown in Fig. 2.3. The sequence of activation starts amongst a group of self-excitatory cells at the top of the right atrium, called the *sinoatrial node*. The action potential wave spreads from this node, causing the atrium to contract, before it reaches the *atrioventricular node*—this is the only pathway for electrical excitation to pass from the atria to the ventricles. From the atrioventricular node, the excitation wave passes to the *Bundle of His*, which conducts the electrical stimulus via the left and right bundle branches into the *Purkinje system* near the bottom of the heart, which transmits the stimulus to the ventricular surface; as the stimulus has thus been transmitted directly from the atria to the bottom of the ventricles, the excitation wave thus spreads upwards through the ventricles, allowing the ventricles to contract from the bottom up as required.

2.1.2 Electrophysiological Properties of Cardiomyocytes

As previously stated, the main rôle of the heart is to serve as a pump to circulate the blood around the body. To do this effectively, it requires coordinated contraction, and this is achieved through the use of coupling the electrical activity of the heart of the mechanical activity (the details of this mechanism will be expanded upon in §2.1.2).

Physically, cardiomyocytes are typically $10 - 20\mu$m in diameter, and $50 - 100\mu$m in length. They are cells bound by a lipid bilayer membrane, separating intracellular space (containing the cytoplasm, nuclei and other organelles) from the extracellular space. The intracellular space has a very different composition to the extracellular space, with the intracellular space containing a high and low concentration of potassium (K^+) and sodium (Na^+) ions respectively; the reverse is true for the extracellular space. These concentration differences are the main reason behind their being a potential difference set up across the cell membrane, referred to as the *membrane potential* (V_m). At rest, due to the high K^+ and low Na^+ in the cell,this potential is negative, though the magnitude varies depending upon the location in the heart; a cardiomyocyte in the ventricles typically has a resting potential (V_{rest})) of about -80mV, while the sinoatrial node has a resting potential of between -50 and -60mV.

Embedded within the bilayer are various membrane-bound proteins which serve to transport ions across the membrane, allowing the membrane to be selectively permeable to particular ions, and allowing regulation of this permeability as required. These transporters can be classed as either *channels* (allow ions to move according to their electrochemical gradient), *pumps* (translocate ions in the opposite direction to their electrochemical gradient by the use of energy) or *exchangers* (translocates a number of ions of one type across the membrane in 'exchange' for a number of ions of another type). Most of these transporters are ion-specific, though some are not exclusively selective. Most of these channels are also controlled by, amongst other things, the membrane potential itself (Bezanilla, 2000). The membrane potential causes a conformational change in the ion channel protein, causing it to 'open' or 'close', that is to allow ions to be conducted through it or not.

These ion channels are discrete molecular entities, and thus the conformational changes that lead to their open/close state are stochastic; the effects of this stochasticity are discussed in greater detail in §2.3. However, each type of ion channel possesses its own range of attributes, such as the time it takes to inactivate, the time it takes to reactivate, its permeability to different types of ions, and its susceptibility to other gating factors. Comprehensive summaries of the properties of ion channels is given in Carmeliet and Vereecke (2002); Roden et al. (2002).

Electrically, the heart can be modelled with great success as an analogue to an electrical circuit (Carmeliet and Vereecke, 2002), where the lipid bilayer is represented as a capacitor, and the various ion channels and transporters that span the membrane are represented as resistors, which change their 'resistance' depending on their state. By altering the resistance of these channels, ion flow across the membrane is permitted via an ionic current. It is a point of nomenclature that an 'inward' current represents the movement of positive ions from the extracellular to the intracellular space, and an 'outward' current is the reverse. This definition is based on the movement on electrical charge, and not on the movement of ion flow. This is subtly different to the definition of an inward or outward rectifier current, where an inward rectifier current passes current more easily inward than outward, and vice versa for an outward rectifier current.

The changes in internal/external ion concentrations which result from these currents changes V_m. The cyclic, periodic change in membrane potential is referred to as the *action potential* (AP). An example of an action potential, showing the different 'phases', is shown in Fig. 2.4.

The AP is considered to consist of 5 different phases, outlined below. The important currents in each phase are mentioned, and greater details are given for a number of these current in §2.1.2.

Phase 4: The resting phase. For ventricular and atrial cardiomyocytes, this phase is marked by a relatively constant value for V_m. The negative resting potential is largely achieved by the inwardly rectifying potassium current (I_{K1}) remaining open

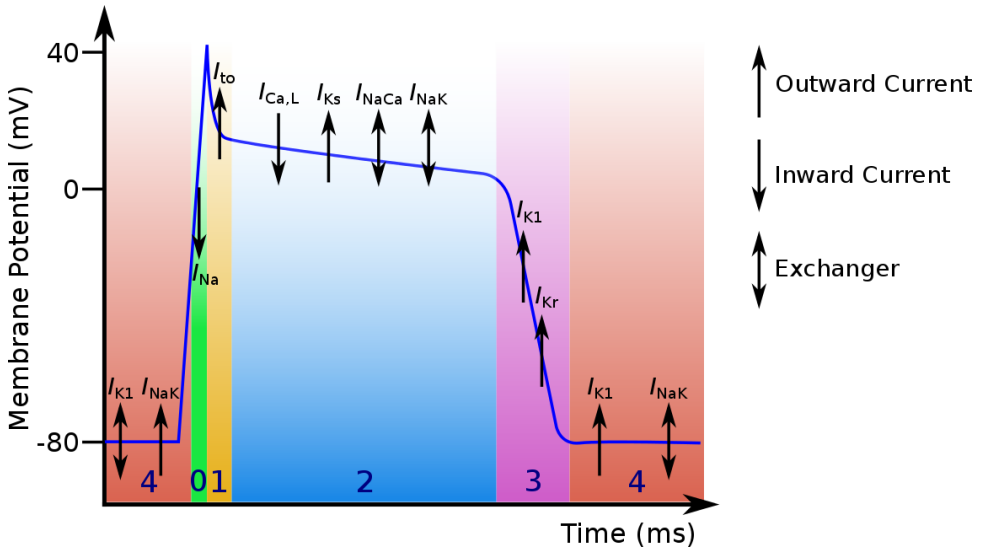

Figure 2.4: *Schematic of a ventricular cardiac AP, with the different 'phases' of the AP shown, and which key currents are involved in each phase. Upward arrows represent outward currents, inward currents represent inward currents, and double arrows represent exchangers,* i.e., *where current moves in both an inward and outward direction.*

during this phase. For pacemaker cells, I_{K1} is absent, and thus the resting phase is actually a period of slow depolarisation, until V_m reaches the threshold value for phase 0. There is also an inward current due to the Na^+-Ca^{2+} exchanger current (I_{NaCa}), which moves 3 Na^+ ions into the cell and one Ca^{2+} ion out at the resting potential.

Phase 0: Period of rapid depolarisation that marks the start of the AP. It is initiated by V_m reaching a threshold value which causes the I_{Na} current to activate, causing a rapid influx of Na^+ into the cell. The direction of I_{NaCa} reverses, and this newly outward current brings in Ca^{2+} and removes Na^+.

Phase 1: Transient repolarisation. The Na^+ channels rapidly deactivate, and the activation of the transient K^+ outward current (I_{to}, occasionally referred to as I_{to1}) results in a period of rapid, partial repolarisation. There may also be a contribution from a Ca^{2+}-activated Cl^-(I_{CaCl}, or I_{to2}). Depending on the strength of this current, this repolarisation may be to the extent that there is a 'notch' in the AP. For example, there is a notch in the AP for ventricular epicardial cells, but no notch for ventricular endocardial cells. The characteristics of this phase are also species-dependent (Carmeliet, 2006).

Phase 2: Plateau phase. The membrane potential is sustained at a relatively constant level by a balance of calcium (Ca^{2+}) influx via the L-type calcium current ($I_{Ca,L}$), and potassium efflux, through the rectifier K^+ currents (rapid,I_{Kr}, and slow, I_{Ks}). Despite being a rapidly activated current, I_{Kr} does not carry large current early during this phase, but only peaks at the end. I_{K1} shows a dramatic fall in conductance during this phase. While most I_{Na} is inactivated during phase 1, there is a small contribution from I_{Na} when V_m is in the limited range where activation and inactivation both occur. Late during phase 2, due to the increase in $[Ca^{2+}]_i$, the reversal potential for I_{NaCa} increases to a value greater than V_m, and thus I_{NaCa} returns to being an inward current.

Phase 3: Repolarisation. The L-type Ca^{2+} current channels close, while the I_{Ks} channels remain open, allowing continuing K^+ efflux resulting in a repolarisation of the cell to the original resting potential. I_{K1} opens during this phase, to remain open during

phase 4 to maintain a steady resting potential.

It should be noted that the above description of which currents act during which phase is only an outline. While the upstroke of the AP is due mostly to the action of I_{Na} and the associated rapid influx of Na^+ ions into the cell, causing the rapid depolarisation, the remaining phases of the AP are more complex, and the failure or part failure of any individual component of the cell mechanism does not necessarily lead to the failure of the whole system. This pseudo-redundancy was first termed *repolarisation reserve* in Roden (1998), and was demonstrated experimentally in Varró et al. (2000). It is essentially the concept that a loss in repolarisation function caused by a reduction or loss of function in one repolarising current can be recovered by increased action of an alternative repolarising current. Most often, this term is applied to K^+ channels, and specifically for the interaction between I_{Kr} and I_{Ks} (Xiao et al., 2008). Several currents are of noted for their rôle in maintaining the repolarisation reserve of the cell, some of which have already been mentioned: I_{Kr}, I_{Ks}, I_{K1}, I_{to}, $I_{\mathrm{Ca,L}}$, I_{Na} (Varró and Baczkó, 2011). The repolarisation reserve is not constant, but rather is dynamic with pacing rate, and variable between species and tissues within the heart (Carmeliet, 2006).

Ion Channel Dynamics

I_{Kr}, as the name implies, is the more rapidly activating of the two rectifier K^+ currents ($\tau \sim 40$ms at $+30$mV), and rapidly activates once V_m increases above -30mV. However, the channel inactivates even more rapidly in a process that precedes voltage-dependent inactivation (Varró and Baczkó, 2011; Spector et al., 1996; Carmeliet, 2006). Due to this, I_{Kr} channels are largely closed during the plateau phase of the AP, only reopening when V_m returns to about 0mV. The transient nature of the current is due to its rapid recovery from inactivation, and subsequent slow deactivation. At slow rates, the contribution of I_{Kr} diminishes further, resulting in a positive feedback look regarding AP duration (APD) lengthening (the same is observed for I_{K1}) (Virág et al., 2009). This same vulnerability of the repolarisation is evident when depolarising factors (*e.g.*, I_{Na}, $I_{\mathrm{Ca,L}}$) are augmented or repolarising factors (*e.g.*, I_{Ks}, I_{K1}) diminished.

If its function is impaired substantially in some way, APD is significantly prolonged by both direct measurements and QT interval measurements in electrocardiograms (ECGs) (the QT interval serves as a marker for the time taken for ventricular depolarisation and repolarisation in a clinical setting), suggesting especial importance in cellular repolarisation (Varró et al., 2000; Lengyel et al., 2001; Jost et al., 2005). When I_{Kr} is only impaired in a minor way, APD may not necessarily increase due to the action of the repolarisation reserve. I_{Kr} is due to a channel encoded by the human ether-á-go-go related gene (HERG), and is known for being its susceptibility to the effects of drug block, making it of key pharmocological importance (Vandenberg et al., 2001; Haverkamp et al., 2000).

I_{Ks} takes longer to activate than its partner (500-1000ms at plateau phase), and deactivates rapidly at negative V_m (Jost et al., 2005; Varró and Baczkó, 2011). Its carries a slowly rising current over the duration of the plateau phase. At rapid pacing rates, the current carried by the I_{Ks} channel increases—this is thought to be due to the kinetics of the channel, with an 'inactivated' state being intermediate between the open and closed state. At rapid pacing rates, there is less time to transition fully to the closed state, and thus there is a greater proportion of I_{Ks} channels available for immediate opening (Silva and Rudy, 2005).

Drug block of I_{Ks} does cause AP prolongation, but not to the same extent as I_{Kr}; while direct measurements show a slight increase in APD, there is very little or no change in QT intervals ECG measurements (Varró et al., 2000; Lengyel et al., 2001; Jost et al., 2005). This implies that its amplitude, compared to that of I_{Kr}, during a typical AP is small—this has been confirmed experimentally under normal conditions (Varró and

Baczkó, 2011). Combined with its slow activation, there is thus relatively little I_{Ks} active during the AP (Jost et al., 2005). However, its long activation time also means the effect of I_{Ks} block is more pronounced APD is prolonged, due to (i) the net outward current at long pacing rates is smaller, so the fractional effect of I_{Ks} is greater, and (ii) more channels are activated during a long AP (Carmeliet, 2006). Due to this action, and the response of I_{Ks} to sympathetic stimulation, the current provides a negative feedback for APD prolongation, acting to curtail the increased action of $I_{\mathrm{Ca,L}}$ that occurs at longer pacing rates. Thus, while under 'normal' circumstances I_{Ks} has limited effect on the repolarisation reserve of the cell, it acts as an effective buffer when APD is longer than normal.

The transmural differences in the expression of I_{Ks} is a large reason behind the transmural variation of APD, and also explains why I_{Kr} block can have a greater or lesser effect, depending on the abundance of the compensatory effect of I_{Ks}(Vandenberg et al., 2001; Carmeliet, 2006). The density of I_{Ks} channels has also been shown to increase in response to sustained I_{Kr} block, demonstrating its importance to the repolarisation reserve (Xiao et al., 2008).

I_{K1} is a strongly inwardly rectifying K^+ current, which means that when V_ms is greater than -30mV, the channel is inactivated. Thus it plays a negligible rôle during the plateau phase of the AP, but has a self-reinforcing role in the repolarisation of the cell once V_m decreases to the extent that I_{K1} can be activated. It should be noted that this is not a voltage-dependent activation, but is based on an unblocking of the channel: when $V_m > -30$mV, the channel is blocked by Mg^{2+} and polyamines which enter the channel from the intracellular side in a voltage-dependent manner. As the current is fully open at V_{rest}, it resists depolarisation caused by either increased pacemaker activity, or Ca^{2+} overload-related delayed afterdepolarisations (DADs). Consequently, I_{K1} may be considered to play an unusual rôle in the repolarisation reserve, and impairment of its function could lead to proarrhythmic effects by making the cell more susceptible to extrasystoles.

I_{to} is actually composed of two separate currents, a rapidly recovering component ($I_{\mathrm{to,f}}$) and a slowly recovering component ($I_{\mathrm{to,s}}$). As a combined unit, it both activates and inactivates rapidly for $V_m > -20$mV, and is of greatest importance during the phase 1 repolarisation. As such, it is believed to have little influence directly on the end repolarisation of the cell, but due to its early role, and its consequent effect on the plateau potential, it is believed to have influence on subsequent currents, which lead to great indirect influence. I_{to} is also known for its transmural variation, being greater in epicardial than endocardial tissue.

I_{NaK} is caused due to the Na^+-K^+ pump, which is an electrogenic exchanger, moving 3 Na^+ ions out of the cell in exchange for 2 K^+ ions. It thus works to maintain the concentration gradients and the resting membrane potential, and provides an outward current in support of the repolarisation reserve. It is, however, sensitive to intracellular Na^+ concentration ($[Na^+]_i$), and consequently to the rate of stimulation.

The influence of $I_{\mathrm{Ca,L}}$ on the repolarisation of the cell is complex due to its complicated inactivation. It inactivates due to voltage slowly, and thus the main reason for its inactivation is due to Ca^{2+}-induced inactivation, and is thus in response to local Ca^{2+} concentration, which is dynamically changing during the plateau phase. This inactivation is modulated via a protein called calmodulin, and thus can be modulated further. If the AP is extended during the range of activation/inactivation for $I_{\mathrm{Ca,L}}$, some $I_{\mathrm{Ca,L}}$ channels may reactivate. This resurgence of the inward current can lead to secondary depolarisations or early after-depolarisations (EADs) (Carmeliet, 2006).

If $I_{\mathrm{Ca,L}}$ (or I_{Na}) are augmented and have their activity increased, this serves to make the plateau potential more positive. While at first glance this may indicate that AP may lengthen, it is rather the case that this may serve to enhance activation of outward K^+

currents, thus shortening APD.

The Na^+-Ca^{2+} exchange current (I_{NaCa}, also referred to as I_{NCX}), like I_{NaCa}, is an electrogenic exchanger, this time exchanging 3 Na^+ ions for one Ca^{2+} ion. By this process, it is, with the SERCA pump, largely responsible for restoring the low cytosolic Ca^{2+} concentration during diastole. It depends strongly on V_m and $[Ca^{2+}]_i$, and thus its magnitude during the AP is difficult to estimate (a problem compounded by the lack a specific inhibitor for the current). It is an outward current at the start of the AP, when V_m and $[Ca^{2+}]_i$ are both low, but then changes to an inward current during the late plateau phase. Due to its sensitivity to $[Ca^{2+}]_i$, in times of Ca^{2+}-overload I_{NaCa} can provide a depolarising current, thus increasing the likelihood of DADs and EADs. The density of I_{Na} is also known to depend heavily on $[Ca^{2+}]_i$, decreasing when $[Ca^{2+}]_i$ is high; the gating of the channel is not affected.

Excitation-Contraction Coupling

Arguably, the complex electrical activity of the AP just described exists for the sole purpose of ensuring the heart acts as an effective mechanical pump. As such, the linking of the electrical activity of the heart to its mechanical contraction is vital, as is referred to as *excitation-contraction coupling*. What follows is a brief summary of the mechanism of this link (the reverse side of this mechanism, termed mechanoelectric feedback, shall not be discussed here).

For this discussion, the cell may be decomposed into units called calcium release units (CRUs), also known as dyads (Cleemann et al., 1998). These CRUs are spread roughly evenly throughout the cell to allow for a uniform action throughout—the number of CRUs in the cell has been estimated to be between 10,000 and 100,000 (Cleemann et al., 1998; Greenstein and Winslow, 2002). Anatomically, the CRU may be considered to be a section of the cell containing a section of the cell membrane, with some L-type Ca^{2+} channels, and a section of the sarcoplasmic reticulum (SR). The primary rôle of the SR is to sequester and release Ca^{2+} via ryanodine receptors (RyRs) when the required stimulus is given. This stimulus is the rise in local concentration of Ca^{2+} precipitated by the opening of the L-type Ca^{2+} current channels, and is termed *calcium-induced calcium release*. The result is that a great deal of Ca^{2+} is released into the cytosol of the cell during phase 2 of the AP. The reason this is vital for ECC is due to the interaction between Ca^{2+} and the contractile units of the cell, called the sarcomere. When the cytosolic concentration of Ca^{2+} ($[Ca^{2+}]_i$) rises, the free Ca^{2+} binds to a part of the contractile machinisms of the cell, which then removes the inhibition between the two critical contractile parts of the mechanism, allowing contraction to take place. Subsequently, the Ca^{2+} released from the SR is recovered by the sarco/endoplasmic reticulum Ca^{2+}-ATPase pumps (Franzini-Armstrong et al., 2005).

2.2 Computational Cell Models

It is often not practicable to test hypotheses in full experimental conditions. In such times, computational/mathematical models have become increasingly important in recent years, as they have developed from their original humble origins. Great advances have been made in accurately modelling individual ion channels, assessing the importance of stochasticity, and probing the interplay between systems and levels in complicated simulations. What follows is a summary of some of the key concepts that are of use in computational models in §2.2.1, and then a brief background on the evolution and development of computational cell models from their early days in §2.2.2. Various difficulties

and problems in model construction that need to be borne in mind when using such models are outlined in §2.2.3.

When considering computational models, it is worth remembering that, from the outset, a model is *wrong* in some way—it is useful insofar as it can answer a posed question. A good model will be able to address a wide range of questions, and will direct future research. This is not necessarily a bad thing—much can be learned from the failure of models, as well as from the success (Noble and Rudy, 2001).

2.2.1 Key Concepts

The model's purpose defines what variables are considered, and how these variables are determined. Some models (*e.g.*, citetRestrepo2008) define a certain section of the cellular mechanism as of interest, and thus the output is defined accordingly. However, most models are trained according to the membrane potential, and thus that is considered the primary output. In modelling the cell as an electrical circuit with the membrane considered as a capacitor, the instantaneous change in membrane potential is calculated according to

$$\frac{\mathrm{d}V_m}{\mathrm{d}t} = -\frac{1}{C_m}(I_{ion} + I_{stim}), \tag{2.1}$$

where C_m is the membrane capacitance, I_{ion} is the sum of all ionic currents in and out of the cell, and I_{stim} is the stimulus current, if applied, to initiate an AP.

In biophysically detailed models of electrically excitable cells, most ionic currents are modelled according to:

$$I_X = g_X(\mathbf{x})(V_m - E_X), \tag{2.2}$$

where I_X represents the ionic current being modelled, $g_X(\mathbf{x})$ represents the conductance of the channel and E_X represents the reversal potential of the cell, which is the potential at which there is no net ion flow through the channel, *i.e.*, there will be no ionic current. The general form of E_X is explained in §2.2.1. $g_X(\mathbf{x})$ is current-dependent variable, and can be modelled as varying with time, voltage, extra-/intracellular ion concentration, etc..

Nernst Potential

Of key importance in mathematical modelling of electrically active cells is the *Nernst equation*. A full derivation is given in the appendix, but the key result is thus:

$$E_X = \frac{RT}{z_X F} \ln \frac{[X]_\mathrm{o}}{[X]_\mathrm{i}} \tag{2.3}$$

In the above equation, R represents the gas constant, z_X represents the valence of ion X, F represents the Faraday constant, and $[X]_\mathrm{o}$ and $[X]_\mathrm{o}$ represent the extracellular and intracellular concentrations of X respectively. The quantity of interest, E_X is the *Nernst potential* or *reversal potential*, and represents the value of V_m required to maintain the intra-/extracellular concentration ratio constant, *i.e.*, to make the net ionic flux across the cell membrane zero.

When a channel is entirely selective, the reversal potential (which can now be thought of as the potential at which there will be no net flux of ions) is given by the Nernst equation for the specific ion. However, some ion channels are permeable to more than one type of

ion, in which case their reversal potential for channel α is given by the *Goldman-Hodgkin-Katz equation*:

$$E_\alpha = \frac{RT}{F} \ln \frac{\Sigma_i^N P_{A_i^+}[A_i^+]_\text{o} + \Sigma_j^M P_{B_j^-}[B_j^-]_\text{i}}{\Sigma_i^N P_{A_i^+}[A_i^+]_\text{i} + \Sigma_j^M P_{B_j^-}[B_j^-]_\text{o}} \tag{2.4}$$

The above equation describes the situation for N different monovalent positive ionic species and M monovalent negative ionic species; different valencies complicate matters further.In it, E_α represents the reversal potential for the channel, *i.e.*, the potential at which, with the given ion concentrations, no net electric flow will occur. The permeability of the membrane is given by P_X; as with the concentrations, the terms have been split into positive (A_i^+) and negative (B_i^-) ionic terms.

Hodgkin-Huxley Current

As previously stated, the seminal work presented in Hodgkin and Huxley (1952) modelled currents as being composed of one of more activation/inactivation gates. It should be noted that the original paper was at pains to emphasise that this was not intended as a description of the actual, physical channel, but was to be used as is: as a mathematical equation that provides a fidelity to the experimental data.

Within this framework, the current conductance can be modelled according to

$$g_X = \overline{g}_X m^a h^b, \tag{2.5}$$

where $\overline{g}_X$ represents the maximum conductance through the channel, a and b are constants, m represents the activation gate and h the inactivation gate. In Hodgkin and Huxley (1952), a physical basis was given to m and h by describing them as proportions of 'activating molecules' and 'inactivating molecules', respectively—the conductance through the channel is thus proportional to the proportion of these molecules that are within and outwith the cell. The variation can thus be described according to

$$\frac{\mathrm{d}m}{\mathrm{d}t} = \alpha_m(1-m) - \beta_m, \tag{2.6}$$

where α_m and β_m are functions of V_m. It can be noted that this is often expressed as

$$\frac{\mathrm{d}m}{\mathrm{d}t} = \frac{m_\infty - m}{\tau_m} \tag{2.7}$$

where $m_\infty = \frac{\alpha_m}{\alpha_m+\beta_m}$ and $\tau_m = \frac{1}{\alpha_m+\beta_m}$, and are the steady state value of m and the time constant, respectively.

At a basic level, in mathematical models of ion channel currents, it is assumed that, instantaneously, they behave like Ohmic resistors, *i.e.*

Markov Models

The Hodgkin-Huxley formulation is computationally efficient, but does not represent a physical reality of the channel state. As such, it is poorly suited to model state specific processes, such as mutation effects or stochasticity. To overcome this, *Markov modelling* can be used (it should be noted that in the formalism presented here, it is not suited to modelling stochastic processes, but can be adapted to do so). Markov modelling works by assuming that the channel can exist in any one of n discrete states. These states can be open, closed or inactivated, and there can be multiple types of each state. The simplest form is a two state system, such as

$$\mathrm{C} \underset{k_{\mathrm{off}}}{\overset{k_{\mathrm{on}}}{\rightleftharpoons}} \mathrm{O},$$

where k_{on} and k_{off} represent the transition rates between these two states—in cardiac modelling, these transition rates typically depend only on the membrane potential. The key requirement for a Markov model is the *Markov property*, which states that the transition to the next state depends only on the current state, and there is no cumulative history of the system that influences its future. Thus, if $x_i(t)$ represents the proportion of channels in state i at time t, and k_{ij} represents the transition rate from state i to state j, the transition rates for a system containing m different states may be modelled according to

$$\frac{\mathrm{d}x_i}{\mathrm{d}t} = \sum_{j=1}^{m}(k_{ji}x_j - k_{ij}x_i). \tag{2.8}$$

The conductance of the channels for a particular current is thus calculated by multiplying the maximum conductance by the proportion of the channels that currently exist in an open state.

2.2.2 Development

What follows is a summary of the progression and development of computational cardiac models. For further details of the models themselves, the reader is referred to the original papers, and for more in depth summaries of the development, the reader is referred to the reviews given in Noble and Rudy (2001); Noble et al. (2012); Noble (2011); Puglisi et al. (2004); Rudy and Silva (2006); Niederer et al. (2009).

The precursor to all computational models of cardiac cells was the model developed in Hodgkin and Huxley (1952). This model described the electrical acitivity of a giant squid axon. It described the ionic currents required to explain the change in membrane potential, using a model for each current of a series of activation and inactivation gating variables (details given in §2.2.1). This model was able to sufficiently model the AP of the neuron using only three ionic currents: a K^+ current, a Na^+ current, and a 'leak' current of other ions. It was further developed by Fitzhugh (1960), which even then recognised that, while the 'truth' of the model was not universally accepted, the model nonetheless was successful in reproducing experimental results. However, FitzHugh was able to demonstrate that, with the correct adaptations of the model equations, the output could be altered to reproduce the longer APs of cardiac cells.

The Hodgkin-Huxley model was hugely successful, and paved the way for the extension of the computational modelling approach to cardiac cells. Preliminary work was shown in Noble (1960), which presented an adaptation of the Hodgkin-Huxley model for the AP of cardiac pacemaker cells. The same 3 currents were used, with adaptations in I_{K} to reproduce the longer AP of cardiac cells. The model was subsequently refined and expanded to reproduce the AP of Purkinje fibre cells (Noble, 1962), taking into account experimental data demonstrating the existence of at least two K^+ currents (labelled I_{K} and I_{K1}) with the resulting change in K^+ permeabilities of the cell membrane (Hutter and Noble, 1960; Carmeliet, 1961; Hall et al., 1963).

This model was followed by a model designed to reproduce the AP of a ventricular myocyte (Krause et al., 1966). The Noble and Krause models were both based on the Hodgkin-Huxley model, with the Noble model being used as the seed for future developments in the computational cardiac modelling field. The next major refinement of the model came with that proposed by McAllister et al. (1975). In response to experimental data, this model greatly expanded the number of ion channels that were being modelled—the previous 4 ODEs of the Noble model were now replaced with 10. This included modelling the componenets of I_{K} separately as I_{Kr} and I_{Ks}, as well as incorporating a Ca^{2+}

current based on experimental recordings from patch clamp experiments. This model, despite its success in reproducing experimental data, also contained an impressive flaw, in that it posited the slow conductance changes near the resting potential to an outward current, activated by depolarisation. In fact, the change was due to an inward current activated by hyperpolarisation (the so-called 'pacemaker current' (I_{F})). Despite this flaw, the overall model remained sound, and iterations of the current continued through to DiFrancesco and Noble (1985), which was the first model to incorporate a formulation for the Na^+-K^+ exchanger, and made most intracellular ion concentrations dynamics. It also managed to model SR Ca^{2+} release, and demonstrated the stoichiometry of the Na^+-Ca^{2+} exchanger had to be 3:1, not 2:1 as had previously been supposed—consequently, the resulting current from this exchange (I_{NaCa}) was incorporated into future models.

While this progress was still being made in the modelling of Purkinje fibre APs, a new focus was found in modelling the AP of ventricular myocytes. While this had already been achieved to some extent in Krause et al. (1966), the first widely used ventricular model was that proposed in the work of Beeler and Reuter (1977). This model was also the first to make more explicit mention of the internal calcium dynamics of the cell, by simulating the Ca^{2+} release from the sarcoplasmic reticulum. Of particular note in the further development of the field is the so-called Luo-Rudy model, first published in Luo and Rudy (1991). This model was originally designed to study arrhythmias in guinea pig ventricular cells, but has been subsequently developed for a wide variety of different tasks, and key components have been adapted into other models for other species (Shaw and Rudy, 1997a,c; Wagner et al., 1999; Viswanathan and Rudy, 1999; Garfinkel et al., 2000; Shannon et al., 2004; Mahajan et al., 2008). Specifically, the model was further adapted in two papers (Luo and Rudy, 1994b,a) to include dynamic intracellular ion concentrations, and $I_{\mathrm{Ca,L}}$ was reformulated. Significantly, I_{K} was separated into the two constituent currents of I_{Kr} and I_{Ks} in Zeng et al. (1995), based on experimental evidence for this separation (Sanguinetti and Jurkiewicz, 1990). The Luo-Rudy model was also adapted to be able to model ischæmia by the incorporation of $I_{\mathrm{K(ATP)}}$ (Shaw and Rudy, 1997b) (further details of the modelling of ischæmia can be found in §2.4.1). A further significant advance came with Clancy and Rudy (1999), which for the first time incorporated Markov modelling into a cell model (Markov modelling is described in greater detail in §2.2.1).

It should be noted that almost all currents in the models described above still use the some basic model form as that given in Hodgkin and Huxley (1952)—details and nuances have been added to some equations, and other equations have been formulated using entirely different methods (*e.g.*, Markov modelling), but the underlying modelling philosophy has remained rather steady, and been found sufficient to the present day.

It is through this evolution of models from relatively humble beginnings that we have reached the point where we are today—computational models of cardiac systems can be used to model anything from the subcellular to the full organ level, with specialisations depending on species, location and situation. In this thesis, focus is mainly devoted to the models presented in Shannon et al. (2004) and Mahajan et al. (2008). These are both models for rabbit ventricular myocytes, with the latter model being itself based on the former—they are both in turn based in large part on the Luo-Rudy model. However, it should not be thought that it is a direct lineage from the Luo-Rudy model to the Shannon model to the Mahajan model—there are numerous intervening steps (Zeng et al., 1995; Puglisi and Bers, 2001; Bassani et al., 2004).

2.2.3 Difficulties in Model Construction

The first difficulty in model construction is perhaps the most obvious: the data used to construct a model is finite—sometimes surprisingly so, especially if the model is designed to reproduce healthy human hearts. But even if the possible problems of limited sample

size are ignored (it is beyond the scope of this thesis to discuss the different possible methods of using data for validation and verification), there are other problems (Marder and Taylor, 2011). As shall be expanded upon further in §2.3, variation is a constant in dealing with experimental data, but methods of dealing with this variation are still being developed. Until recently, a model would be designed to reproduce the 'data', without reproducing the variation. The choice of what 'data' to fit was therefore important, and yet fraught with difficulties. For example, should one fit to the maximum measured value on the basis that voltage-clamp experiments tend to make the currents appear smaller and slower than they are, or should one fit to the mean value in order to use a greater range of data? Both approaches have problems, not least that a model with mean parameters can fail to have properties exhibited by all of the test subjects (Golowasch et al., 2002; Marder and Taylor, 2011).

A further problem comes with unknown parameters—even in well-studied systems, there are parameters that, for whatever reason, are not well-defined. There are two possible options to deal with this: (1) adopt a parameter derived from a similar system, *e.g.*, the peak conductance used in a model for a different species, or (2) adjust the parameter on the basis of producing the expected output (so-called *phenomenological fitting*). This problem is especially prevalent for fitting parameters that describe peak/maximum conductance of ion channels. In voltage clamp experiments, this is often the most poorly defined parameter, due to both the detrimental effects of the initial cell isolation procedure on ion channels, and due to the drug block used to try and isolate particular ion channels for measurement being either incomplete or non-specific.

Further difficulties can arise when fitting data due to the experimentally verified repolarisation reserve. While this is a genuine physical phenomenon, when fitting parameters for a computational model, it is possible that, due to the relations between currents and ion concentrations, the model may present with a wide range of possible values that fit the experimental data, with the computational repolarisation reserve being very different to the physiological repolarisation reserve.

2.3 Variation

Stochasticity has been mentioned in passing already in this dissertation. Stochasticity, and more generally variation, is now being recognised as being of key importance in many biological questions. Variation exists at all ranges, and at all scales—if one wished to be pedantic, one could point to the probabilistic collapse of the quantim wavefunction as the seed for all uncertainty, but there is no current evidence that quantum effects play any rôle in cardiac function. However, variation does exist, and accounting for it is becoming an increasingly important aspect of cardiac modelling.

In §2.3.1, the various possible sources and problems of variation in biological settings are discussed, and in §2.3.2, the various methods used so far to address this variation in computational models are outlined.

2.3.1 Experimental & Physiological Variation

As stated, variation exists at all scales, both temporally and spatially: from individual ion channels, to the level of the cell, to tissue, to organ, and to organism. At the scale of ion channels, variation has been noted in the mRNA concentrations that are translated to functional ion channels (Gaborit et al., 2007). While it has been noted that mRNA levels do not translate directly to ion channel concentrations for numerous reasons (Edelman and Gally, 2001; Nattel et al., 2010), a link has still be demonstrated between mRNA

levels and observable effects on the AP (Walmsley et al., 2013). There is also a substantial body of evidence for notable variation in cellular processes—in neuronal studies, maximal conductance of ion channels has been shown to vary substantially (Marder and Taylor, 2011; Goaillard et al., 2009; Schulz et al., 2006), both in theoretical and experimental studies.

As has previously been commented upon, there are notable differences in cellular APs depending the the spatial location on the cell—this is evident from variation between ventricular and atrial (and other) cardiac cells (Carmeliet and Vereecke, 2002), to transmural variation (Antzelevitch et al., 1991). Furthermore, temporal variation is also a common phenomenon (Walmsley et al., 2010). At the organ level, numerous factors have been cited as having notable effects on the AP (Taylor and Lipsitz, 1997). At the organismal level, different individuals react differently to different therapies (Kannankeril et al., 2010). After considering all these changes, there are still notable differences that can be attributed to gender, age, and experimental method.

A complete and comprehensive discussion of experimental variation is beyond the scope of this dissertation. However, mention shall be made for the experimentally observed variation that is of note for the models and experiments contained within this thesis. The complete gamut of experimental values is almost impossible to find—rather, some measure of the experimental range can be ascertained from the literature by the error values given, which represent the standard deviation of the results from the presented mean value.

Action Potential Variation

Collaborators from the University of Szeged have been able to obtain AP traces for ventricular tissue at pacing rates of 600ms and 1,000ms. These preparations are internally consistent—the trace for each preparation comes from a single sample (although the electrode recording the potential occasionally lost contact, and thus had to be reapplied, thus leading to the recording not necessarily coming for the same individual myocyte). These valuable data allow assessment of the intra-preparation variation in AP, and inter-preparation variation. Using data for APD_{90} (arguably the most common AP metric), these data suggest an intra-preparation variability of $\sim 3.5\%$, and an inter-preparation variability of $\sim 10\%$.

However, these data come from a single laboratory—a full literature review provides a much greater range of values. From these results, it is possible to generate a range of APD_{90} values that can be regarded as physiologically realistic. While many of these values come from tissue preparations, preliminary experiments with the Mahajan model suggest that there is little difference between cellular and tissue results for APD_{90}. The results of such a literature search gives the physiological range for APD_{90} to be $142 - 185$ms for a basic cycle length (BCL) of 400ms, $160 - 220$ms for a BCL of 600ms, and $167 - 230$ms for a BCL of 1,000ms (Biagetti and Quinteiro, 2006; Szigligeti et al., 1996; Yan et al., 2001; Jung et al., 2011; Goldhaber et al., 2005; Wu et al., 2011; Chen et al., 2006; Kirchhof et al., 2003; Eckardt et al., 1998; Zabel et al., 1997b,a; Kurz et al., 1993; McIntosh et al., 2000).

Ion Channel Variation

Many experiments, aware of the added variation associated with differences in gender and age, pick the experimental test subjects to be as homogeneous as possible. Even with that, notable variations can be found. Fülöp et al. (2004) used experimental data to determine properties of $I_{\mathrm{Ca,L}}$, and found (amongst other details) that the density of peak

Current	Location	Value ($pApF^{-1}$)	Percentage Variation
I_{to}	Apex	29.6±5.7	±19.3%
	Base	16.5±4.4	±26.6%
$I_{Ks,peak}$	Apex	5.61±0.43	±7.7%
	Base	2.14±0.18	±8.4%
$I_{Ks,tail}$	Apex	1.65±0.21	±12.7%
	Base	0.85±0.19	±22.4%
$I_{Ca,L}$	Apex	−5.85±0.76	±13.0%
	Base	−7.17±0.63	±8.8%

Table 2.1: *A summary of the results for the current densities of basal and apical ventricular tissue in human and canine myocytes and tissue, obtained from Szentandrássy et al. (2005).*

$I_{Ca,L}$ in human ventricular myocytes was $-5.5 \pm 0.4 pApF^{-1}$ (±7.27%). Similar values were obtained by Li et al. (1999), with even greater variation reported for plateau $I_{Ca,L}$ (up to 18.2%). In the work of Fink et al. (2008), by fitting to experimental data, g_{K1} was determined to be $0.5871 \pm 0.0503 pApF^{-1}mV^{-1}$.

Notable work has also been carried out in Szentandrássy et al. (2005), which examined the amplitude (and time constants) of several ion channel currents in human and canine tissue to study the inhomogeneities between basal and apical ventricular tissue—a summary of these results is given in Table 2.1. It can be seen that the individual results demonstrate significant variation, and variation between apical and basal values is often noteworthy.

The effect of gender is addressed in humans in Verkerk et al. (2005), and in rabbits in Sims et al. (2008), which also examines the effect of age. The data for humans is not statistically significant, but still shows consistent bias. For example, $I_{Ca,L}$ density in female ventricular myocytes is consistently greater than in male at all voltages (*e.g.*, 129% at 0mV) and for I_{to}, female I_{to} density at 50mV is 84% of the male. The individual measurements in Sims et al. (2008) show up to 9.4% variation in individual measurements, but the gender difference can be far greater—from 22% in prepubertal rabbit ventricular myocytes, to 32% in adult myocytes extracted from the base of the ventricle.

2.3.2 Computational Modelling of Variation

It is a handicap that is only recently being overcome that, in constructing cell models, the focus is one fitting the model output to one particular value, whether this is the mean or some other measure. As such, these models are often poorly equipped to reproduce the variation that is seen in the original experimental data.

When modelling variation, it must be remembered once again that models are only useful up to the point of answering the question posed to them—taking a model further than its original purpose is useful only when this new purpose does not stray irrevocably from the original. As such, reproduction of variation using existing computational models is fraught with difficulties when translating the results to the real system. For example, in work by Davies et al. (2012), it was shown that by allowing parameters describing peak ion channel conductance to vary, a wide range of possible values could be made to fit experimental AP, with peak conductance varying from as little as 0.1 to as much as 7.43 of the original model's peak conductance value. However, this demonstrates one possible problem in simply fitting parameters: numerically, it may well be entirely accurate, but it may not represent physiological reality (experimental data for conductance variation implies a variation of as much as threefold (Schulz et al., 2006)).

As a tangent to this problem of maintaining the link between reality and model, it has been shown that, under particular conditions, a computational model can produce identical AP traces while using two vastly different input parameter sets (Sarkar and Sobie, 2010). However, these models produce very different data for $[Ca^{2+}]_i$. Obviously, if the model is required only to reproduce the AP, both models are entirely adequate. However, the problem is demonstrated further in Cherry and Fenton (2007) in a comparison between two different canine ventricular models: while both produce APs of similar morphologies, there are significant underlying differences, and these are reflected in different responses to certain conditions. Similar conclusions have been reached in Romero et al. (2011), and work has been made in finding some way of curating models according to their differences in response (Terkildsen et al., 2008; Cooper et al., 2011).

It is generally felt that a 'good' model should be able to reproduce a wide range of data (it is sometimes, unfortunately, difficult to get as wide a data range as one would like). If a biophysically detailed model can reproduce a wide range of data, it gives us greater confidence that the underlying details of the model can be said to represent reality. By combining a consideration of the model response to different conditions with data regarding the model response to variation, a model's accuracy and efficacy may be assessed, and new experimental directions suggested to either determine which of certain models' hypotheses regarding cell mechanics is accurate, or to elucidate other questions raised.

The interplay between input parameters and output parameters is decidely non-linear, and the effects of changes in one, or many parameters, cannot easily be predicted (Sarkar et al., 2012); this is illustrated in Fig. 2.5. The previous modelling paradigm has been to consider the model as occupying a single point in the input/output parameter space—this is represented by the blue point in the figure. However, it is becoming increasingly prevalent to consider variation in both input and output parameter space, represented by the cloud of red points in the figure. However, the mapping between the input and output spaces is non-linear, and there is no guarantee that a point in the middle of the input cloud translates to a point in the middle of the output cloud, or even if the clouds are the same shape (as shown in the figure). Furthermore, the problem increases in complexity as one considers more input parameters and output metrics.

There are many different ways to try and elucidate this input/output mapping. One of the more common methods has been *parameter sensitivity analysis*, which varies an individual input parameter at a time to elucidate the effect this parameter has on a given set of output metrics, and expressing this effect in a quantitative manner (*i.e.*, Δoutput/*Delta*parameter). This work successfully indicates which parameters are most directly responsible for which output metric (Nygren et al., 1998; Romero et al., 2009, 2010; Corrias et al., 2011; Romero et al., 2011). This method (and many of the following methods) has obvious extensions to computational predictions for pharmocological ion channel block.

An elegant extension of this method was demonstrated in Sobie (2009). This presented a computationally efficient method to analyse the effects of multi-parameter variation. For a given set p of input parameters (*e.g.*, g_{NaK}, τ_{NaK}, etc.), a range of possible values for each parameter is defined. This could be based on a percentage range, *e.g.*, $\pm 15\%$, or based on the range observed for a given parameter in the literature, or any other number of methods. From this possible range of different parameters, a multitude of different parameter sets can be selected. A sample of size n is selected, models using these parameter sets are simulated, and the result of these models is recorded according to m output metrics (*e.g.*, APD_{90}, $[Ca^{2+}]_i^{\mathrm{sys}}$, etc.). Before further analysis, the data are mean-centred and normalised by the standard deviation, *i.e.*, $x_{\mathrm{new}} = (x_{\mathrm{orig}} - \mu_x) - \sigma_x$, where x_{new} and x_{orig} are the new and original data values, and μ_x and σ_x are the population mean and standard deviation for the data, respectively.

The data are now organised into matrices: the input parameter data are organised into

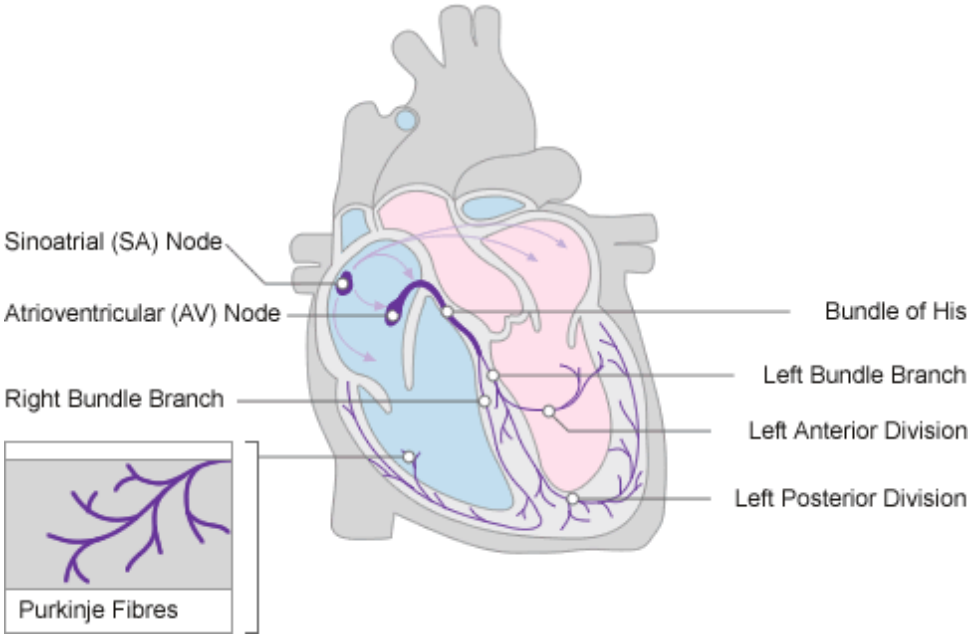

Figure 2.5: *Illustration of the effect of possible parameter variation on model output. In this example, two given input parameters (p_1 and p_2) have a complicated effect on two measured outputs of the model (o_1 and o_2); one possible example data point is highlighted in blue. Based on a figure from Sarkar et al. (2012).*

an input $n \times p$ matrix ($\mathbf{X}$), and the output metric data are organised into a $n \times m$ output matrix ($\mathbf{Y}$). Each column thus represents one of the input parameters/output metrics, and each row represents one of the parameter sets simulated, and the resulting output. Multivariable regression analysis is then used to derive the effect matrix $\mathbf{B}$ such that

$$\mathbf{XB} = \hat{\mathbf{Y}} \approx \mathbf{Y}, \tag{2.9}$$

where $\hat{\mathbf{Y}}$ is a close approximation of $\mathbf{Y}$. The result of this analysis is the $p \times m$ matrix of regression coefficients, and has been utilised as each row representing the effect of a given input parameter on the numerous output metrics, and each column representing the effect of various input parameters on a particular output metric. This has been shown to be successful in predicting the output of a new parameter set (Sobie, 2009), but has also been used to replicate the results of the original parameter sensitivity analysis, *i.e.*, to demonstrate the effect of a series of input parameters on a given output metric. This method has been used to investigate the effect of such variability on the repolarisation reserve (Sarkar and Sobie, 2011), and also to investigate the possible range of variability in a given set of parameters given the experimentally observed variation in certain output metrics by reversing the regression analysis (*i.e.*, calculating $\mathbf{B}$ such that $\mathbf{X} \approx \hat{\mathbf{X}} = \mathbf{YB^{-1}}$) (Sarkar and Sobie, 2010).

This method is an elegant method of investigating the effect of multiple parameter variation on multiple model outputs. However, it should be noted that this method still, to some degree, reduces the multi-dimensional parameter variation to a single-dimensional result. The interactions are still tested, and are thus present in an intrinsic sense in the resulting matrix $\mathbf{B}$. However, extracting these interactions in an explicit manner is not so simple, and thus the results of the multi-dimensional parameter variation are, in effect, reduced to the result of a single-dimensional parameter variation. It should also be noted that, due to the non-linear effect ion concentrations have on ion-voltage relations, the accuracy of this method may be reduced when concentrations are also allowed to vary. The effect of pacing rate has also not been addressed.

An alternative method is to take advantage of so-called genetic algorithms to tune models to given experimental data. This has been used to provide single parameter sets, and adapt models to new data (Kherlopian et al., 2011). It has also been successfully adapted to find multiple parameter sets that reproduce experimental data, where the parameter sets are not considered part of a continuum of models, with minor variations accounting for the different sets (Achard and De Schutter, 2006; Syed et al., 2005). While that work reproduced a single set of experimental data, it is not unreasonable to expect this method to be easily adapted to reproduce a range of experimentally observed values.

The effects of multiple parameter variation can also be addressed via a comprehensive parameter sweep (this approach has also been referred to as a database method). The guiding principle of such a method is to comprehensively examine a given parameter space—for example, if the effect of variation in p different parameters is being investigated, the model is simulated for every single possible combination of these parameters. If there are q different possible values for each parameter, this leads to p^q different simulations that would be run, unless measures are taken to limit this by some means (such as by taking advantage of experimentally demonstrated correlations between parameters (Schulz et al., 2006)). While this method can be computationally expensive, such a parameter search is also often embarrassingly parallel, and thus can be performed rapidly in real-time using such facilities as the Nimrod computing system (Abramson et al., 2000, 1997, 2010).

The parameter sweep method was first used in Prinz et al. (2003), which applied variation to eight maximal conductances in a model of a lobster stomatogastric neuron to generate a database of about 1.7million different models, and then classified these models according to their activity pattern. This database could then be searched for different models that satisfied a prescribed set of criteria. Similar work has been carried out to investigate CICR (Sobie and Ramay, 2009). Indeed, there is increasing traction for replacing the previous paradigm of a single parameter set with a single model with a parameter 'space' for a model, leading to a population of models (Davies et al., 2012; Taylor et al., 2009; Prinz et al., 2003; Marder and Taylor, 2011)

2.4 Cardiac Disease

Cardiac disease is a costly condition for Western countries, but the pathology of such diseases can often be complicated. In-depth analysis of the mechanisms for disease is vital in determining how to treat diseases at a more fundamental level than symptomatically. As such, research has demonstrated many causal links between the cellular mechanisms, such as ion channels and their links to pacing rate, etc., and pathologies (Inoue et al., 2006; Kurz et al., 1993; Rodríguez et al., 2006; Dumaine et al., 1996; Nattel et al., 2010; Jurkat-Rott and Lehmann-Horn, 2005; Biagetti and Quinteiro, 2006).

Using the multi-parameter matrix regression method, it is possible to simulate the effects on the model output of the known changes in input parameters in disease conditions. The data from the effect matrix $\mathbf{B}$ can then be used to determine which of the parameter changes causes which effect on the output, and to what degree (Sarkar et al., 2012).

As with computational modelling in general, the importance of the possible effects of variation are coming into focus in disease modelling as well. The focus in this dissertation thus far has been on the importance of modelling variation to gain insight into the mechanics underlying cellular processes, and the different methods that have been used in this goal thus far. However, one key area of work is not just to understand variability under normal conditions, but under pathological conditions—it has already been established that variation can have significant, meaningful effects to the outcome of pathological conditions, either by exacerbating or ameliorating the condition (Sarkar et al., 2012; John et al., 2012). For example, a particular variation can lead to either an

increase or a reduction in the repolarisation reserve. The possible consequences of the changes that this variation could lead to are significant, not least due to providing a key to understanding the differing responses to different therapies, including the effects of drug block.

A leading area of research to that effect has been on drug-induced Long QT Syndrome (diLQTS). Drug-induced or not, LQTS represents a condition where repolarisation is extended; the name derives from the prolongation of the QT interval on an ECG. Where LQTS is drug-induced, the most common causative drug is one that blocks the action if I_{Kr} (in the literature, this may also be referred to as HERG block, named after the gene that produces the channel). However, not only is the response to I_{Kr}-blocking drugs variable (Kannankeril et al., 2010), but the degree of response appears uncorrelated with baseline ECG recordings. The causes for these differences are only beginning to be elucidated, but it has been theorised that it may be due to differing repolarisation reserves (Varró and Baczkó, 2011), which in turn may be due to variation—variation which may be amenable to computational modelling (it should be noted that drug effects are subject to variation at many levels, and the variation that has been the subject of this dissertation—ion channel variation—is only one). Novel work has been performed in Sarkar and Sobie (2011) to investigate the link between different input parameter values and the resulting change in output when drug block is simulated.

2.4.1 Ischæmia

Despite what would be expected from the Nernst equation, increased extracellular K^+ is known to enhance I_{Kr} (Sanguinetti and Jurkiewicz, 1992; Yang et al., 1997)

Diffusion

This appendix gives greater detail about the ionic movement theories, and electric theory properties generally, of the modelling of electrically active cells—note that this applies equally well to both cardiac cells and to neurons.

A.1 Simple Diffusion

By simple diffusion, there is a net movement of particles from a region of high concentration to a region of low diffusion with simple thermal movement. This movement is according to Fick's Law,

$$F_X = -D\frac{\partial C_X}{\partial x}, \tag{A.1}$$

where F_X and C_X represent the flux and concentration of particle X respectively, and D represents the diffusion coefficient. It should be noted that this represents *net* diffusion: there will be movement of particles in both directions. For circumstances where D is constant, this solves to produce

$$F_X = P(C_{X,o} - C_{X,i}), \tag{A.2}$$

where P represents the permeability of the membrane, and is equivalent to $^{\mathrm{D}}/_{\mathrm{d}}$, where d represents the thickness of the membrane. $C_{X,o}$ and $C_{x,i}$ represent the extracellular and intracellular concentrations of X, respectively; thus F_X in this form describes flux from the extra- to the intracellular space. It can be noted that for substances that diffuse through the lipid phase of the membrane, the permeability also depends on the oil/water partition coefficient β, according to $P = \beta^{\mathrm{D}}/_{\mathrm{d}}$.

A.2 Facilitated Diffusion, Michaelis-Menten Kinetics

While Fick's Law can describe the movement of small, uncharged particles and some ions across a membrane very well, it does not serve particularly well for large molecules or charged substances. While ions can move across the membrane via membrane proteins suchs as channels and exchangers, some large molecules such as amino acids and

glucose are large enough that pore-based channels would have no selectivity over what moves through them. Thus, they instead make use of *carrier-mediated diffusion*, also called *facilitated diffusion*, where the molecule binds to a transmembrane protein and causes a conformational change that results in the molecule being translocated across the membrane.

This mechanism obeys Michaelis-Menten kinetics, and can be views as a catalysed reaction, where the reaction is not a chemical one, but rather a translation of substance across the membrane.

Briefly, Michaelis-Menten kinetics are used to describe a two-stage reaction, the first stage being reversible, the second stage irreversible:

$$\mathrm{C} + \mathrm{X_o} \rightleftharpoons \mathrm{CX} \longrightarrow \mathrm{C} + \mathrm{X_i}$$

The above expression uses $\mathrm{X_o}$ and $\mathrm{X_i}$ to represent the extracellular and intracellular molecule respectively, and C the carrier; CX represents the moment when the molecule and the carrier combine for the transport process. It thus proposes that there is a reversible reaction between the extracellular molecule and the carrier, and that the transport process itself is irreversible. By certain assumptions, including that the number of extracellular molecules is far greater than the number of carriers, the rate of this process can be estimated to be

$$v = \frac{\mathrm{d}\mathrm{X_o}}{\mathrm{d}t} = v_{\max}\frac{[\mathrm{X_o}]}{K_m + [\mathrm{X_o}]}, \tag{A.3}$$

where v represents the velocity of the reaction (*i.e.*, the rate of translocation of X), $v_{\max}$ represents the maximum velocity at which the translocation can take place, $[\mathrm{X_o}]$ the concentration of X outside the cell, K_m represents the so-called Michaelis-Menten constant, which in turn represents the concentration at which the half-maximum speed occurs. It can be noted that $v_{\max}$ is equal to the rate of the final step of the reaction.

Facilitated diffusion shows saturation (the point at which increasing the extracellular concentration further does not lead to an increase in flux), competitive and non-competitive inhibition, stereo-specificity and a relatively slow turnover.

A.3 Electrodiffusion

This section deals with the form of transportation that is of most interest for this thesis: the passive movement of charged substances (ions) in the presences of an electrochemical gradient. It should be noted that the content in this section, while being in the appendix, is nonetheless vital for almost all mathematical models of electrically active cellular activity.

A.3.1 The Nernst Equeation

A key concept is that of the *Nernst Potential*, derived using the Nernst Equation, which describes the potential difference that is required to oppose the net flow of an ionic species against a specified concentration gradient. The equation shall here be derived in full using statistical mechanics.

Initially, recall that the probability of a system being in a particular state α is given by

$$P(\alpha) = \frac{1}{Z}e^{-\beta E_\alpha}; \qquad Z = \sum_i e^{\beta E_i}, \tag{A.4}$$

where E_i is the energy of state i, and $\beta = k_\mathrm{B}T$, with T being the temperature of the system.

For a large number of molecules, $[A] \propto P(A)$. Furthermore, if we consider the diffusion of ions from one location to another to be a reversible reaction according to $\mathrm{A} \underset{k_2}{\overset{k_1}{\rightleftharpoons}} \mathrm{B}$, by applying the law of mass action ($F_{A\to B} \propto [A]$), at steady state we achieve the following equation, which can be manipulated accordingly:

$$k_1[A] = k_2[B] \tag{A.5}$$

$$\frac{[A]}{[B]} = \frac{k_2}{k_1} \tag{A.6}$$

$$= \frac{\frac{1}{Z}e^{-\beta E_A}}{\frac{1}{Z}e^{-\beta E_B}} \tag{A.7}$$

$$= e^{-\beta(E_A - E_B)} \tag{A.8}$$

$$\Delta E = k_\mathrm{B}T \ln \frac{[B]}{[A]} \tag{A.9}$$

At this stage, the electric gradient is introduced to the equation as the reason for the energy difference that maintains the steady state, with $\Delta E = zqV$, where z is the valence of the ionic species being considered, q_e is the charge (in this case equal to the charge of an electron, *i.e.*, the charge of a singly ionised ion), and V is the potential difference.

$$zq_eV = k_\mathrm{B}T \ln \frac{[B]}{[A]} \tag{A.10}$$

$$V = \frac{k_\mathrm{B}T}{zq_e} \ln \frac{[B]}{[A]} \tag{A.11}$$

$$= \frac{RT}{zF} \ln \frac{[B]}{[A]} \tag{A.12}$$

$$\tag{A.13}$$

Equations A.11 and A.12 are equivalent, the only difference being the constants used in the expression. Eq. A.12 is the more common formulation, using the gas constant R and the Faraday constant F in place of the Boltzmann constant k_B and the electron charge q_e respectively. The Nernst potential is, therefore, the potential difference that must be applied to maintain a specified concentration gradient, and is given by either equation.

Bibliography

Abramson, D., Bernabeu, M. O., Bethwaite, B., Burrage, K., Corrias, A., Enticott, C., Garic, S., Gavaghan, D., Peachey, T., Pitt-Francis, J., Pueyo, E., Rodríguez, B., Sher, A., and Tan, J. (2010). High-throughput cardiac science on the Grid. *Philosophical Transactions. Series A, Mathematical, Physical, and Engineering Sciences*, 368(1925):3907–23.

Abramson, D., Foster, I., Giddy, J., Lewis, A., Sosic, R., Sutherst, R., and White, N. (1997). The Nimrod Computational Workbench : A Case Study in Desktop Metacomputing. *Proceedings of the 20th Australasian Computer Science Conference*.

Abramson, D., Giddy, J., and Kotler, L. (2000). High Performance Parametric Modeling with Nimrod / G : Killer Application for the Global Grid? In *International Parallel and Distributed Processing Symposium (IPDPS)*, pages 520–528, Cancun, Mexico.

Achard, P. and De Schutter, E. (2006). Complex parameter landscape for a complex neuron model. *PLoS computational biology*, 2(7):e94.

Antzelevitch, C., Sicouri, S., Litovsky, S. H., Lukas, A., Krishnan, S. C., Di Diego, J. M., Gintant, G. a., and Liu, D. W. (1991). Heterogeneity within the ventricular wall. Electrophysiology and pharmacology of epicardial, endocardial, and M cells. *Circulation Research*, 69(6):1427–1449.

Bassani, R. A., Altamirano, J., Puglisi, J. L., and Bers, D. M. (2004). Action potential duration determines sarcoplasmic reticulum Ca2+ reloading in mammalian ventricular myocytes. *The Journal of Physiology*, 559(Pt 2):593–609.

Beeler, G. W. and Reuter, H. (1977). Reconstruction of the Action Potential of Ventricular Myocardial Fibres. *The Journal of Physiology*, 268:177–210.

Bezanilla, F. (2000). The voltage sensor in voltage-dependent ion channels. *Physiological Reviews*, 80(2):555–92.

Biagetti, M. O. and Quinteiro, R. A. (2006). Gender differences in electrical remodeling and susceptibility to ventricular arrhythmias in rabbits with left ventricular hypertrophy. *Heart Rhythm : the Official Journal of the Heart Rhythm Society*, 3(7):832–9.

Carmeliet, E. (1961). Chloride ions and the membrane potential of Purkinje fibres. *The Journal of Physiology*, 156:375–388.

Carmeliet, E. (2006). Repolarization Reserve in Cardiac Cells. *Journal of Medical and Biological Engineering*, 26(3):97–105.

Carmeliet, E. and Vereecke, J. (2002). *Cardiac Cellular Electrophysiology*. Springer.

Chen, X., Cordes, J. S., Bradley, J. A., Sun, Z., and Zhou, J. (2006). Use of arterially perfused rabbit ventricular wedge in predicting arrhythmogenic potentials of drugs. *Journal of Pharmacological and Toxicological Methods*, 54(3):261–72.

Cherry, E. M. and Fenton, F. H. (2007). A tale of two dogs: analyzing two models of canine ventricular electrophysiology. *American journal of physiology. Heart and circulatory physiology*, 292(1):H43–55.

Clancy, C. E. and Rudy, Y. (1999). Linking a genetic defect to its cellular phenotype in a cardiac arrhythmia. *Nature*, 400(6744):566–9.

Cleemann, L., Wang, W., and Morad, M. (1998). Two-dimensional confocal images of organization, density, and gating of focal Ca2+ release sites in rat cardiac myocytes. *Proceedings of the National Academy of Sciences of the United States of America*, 95(18):10984–9.

Cooper, J., Mirams, G. R., and Niederer, S. a. (2011). High-throughput functional curation of cellular electrophysiology models. *Progress in biophysics and molecular biology*, 107(1):11–20.

Corrias, A., Giles, W., and Rodriguez, B. (2011). Ionic mechanisms of electrophysiological properties and repolarization abnormalities in rabbit Purkinje fibers. *American journal of physiology. Heart and circulatory physiology*, 300(5):H1806–13.

Davies, M. R., Mistry, H. B., Hussein, L., Pollard, C. E., Valentin, J.-P., Swinton, J., and Abi-Gerges, N. (2012). An in silico canine cardiac midmyocardial action potential duration model as a tool for early drug safety assessment. *American Journal of Physiology. Heart and Circulatory Physiology*, 302(7):H1466–80.

DiFrancesco, D. and Noble, D. (1985). A Model of Cardiac Electrical Activity Incorporating Ionic Pumps and Concentration Changes. *Philosophical Transactions of the Royal Society B: Biological Sciences*, 307(1133):353–398.

Dumaine, R., Wang, Q., Keating, M. T., Hartmann, H. A., Schwartz, P. J., Brown, A. M., and Kirsch, G. E. (1996). Multiple mechanisms of Na+ channel–linked long-QT syndrome. *Circulation Research*, 78(5):916–24.

Eckardt, L., Haverkamp, W., Göttker, U., Madeja, M., Johna, R., Borggrefe, M., and Breithardt, G. (1998). Divergent effect of acute ventricular dilatation on the electrophysiologic characteristics of d,l-sotalol and flecainide in the isolated rabbit heart. *Journal of Cardiovascular Electrophysiology*, 9(4):366–83.

Edelman, G. M. and Gally, J. a. (2001). Degeneracy and complexity in biological systems. *Proceedings of the National Academy of Sciences of the United States of America*, 98(24):13763–8.

Fink, M., Noble, D., Virág, L., Varró, A., and Giles, W. R. (2008). Contributions of HERG K+ current to repolarization of the human ventricular action potential. *Progress in Biophysics and Molecular Biology*, 96(1-3):357–76.

Fitzhugh, R. (1960). Thresholds and plateaus in the Hodgkin-Huxley nerve equations. *The Journal of general physiology*, 43:867–96.

Franzini-Armstrong, C., Protasi, F., and Tijskens, P. (2005). The assembly of calcium release units in cardiac muscle. *Annals of the New York Academy of Sciences*, 1047:76–85.

Fülöp, L., Bányász, T., Magyar, J., Szentandrássy, N., Varró, A., and Nánási, P. P. (2004). Reopening of L-type calcium channels in human ventricular myocytes during applied epicardial action potentials. *Acta Physiologica Scandinavica*, 180(1):39–47.

Gaborit, N., Le Bouter, S., Szuts, V., Varró, A., Escande, D., Nattel, S., and Demolombe, S. (2007). Regional and tissue specific transcript signatures of ion channel genes in the non-diseased human heart. *The Journal of Physiology*, 582(Pt 2):675–93.

Garfinkel, A., Kim, Y. H., Voroshilovsky, O., Qu, Z., Kil, J. R., Lee, M. H., Karagueuzian, H. S., Weiss, J. N., and Chen, P. S. (2000). Preventing ventricular fibrillation by flattening cardiac restitution. *Proceedings of the National Academy of Sciences of the United States of America*, 97(11):6061–6.

Goaillard, J.-M., Taylor, A. L., Schulz, D. J., and Marder, E. (2009). Functional consequences of animal-to-animal variation in circuit parameters. *Nature neuroscience*, 12(11):1424–30.

Goldhaber, J. I., Xie, L.-H., Duong, T., Motter, C., Khuu, K., and Weiss, J. N. (2005). Action potential duration restitution and alternans in rabbit ventricular myocytes: the key role of intracellular calcium cycling. *Circulation Research*, 96(4):459–66.

Golowasch, J., Goldman, M. S., Abbott, L. F., and Marder, E. (2002). Failure of averaging in the construction of a conductance-based neuron model. *Journal of Neurophysiology*, 87(2):1129–31.

Greenstein, J. L. and Winslow, R. L. (2002). An integrative model of the cardiac ventricular myocyte incorporating local control of Ca2+ release. *Biophysical Journal*, 83(6):2918–45.

Hall, A. E., Hutter, O. F., and Noble, D. (1963). Current-Voltage Relations of Purkinje Fibres in Sodium Deficient Solutions. *The Journal of Physiology*, 166:225–240.

Haverkamp, W., Breithardt, G., Camm, a. J., Janse, M. J., Rosen, M. R., Antzelevitch, C., Escande, D., Franz, M., Malik, M., Moss, A., and Shah, R. (2000). The potential for QT prolongation and pro-arrhythmia by non-anti-arrhythmic drugs: clinical and regulatory implications. Report on a Policy Conference of the European Society of Cardiology. *Cardiovascular research*, 47(2):219–33.

Hodgkin, A. L. and Huxley, A. F. (1952). A quantative description of membrane current and its application to conduction and excitation in nerve. *The Journal of Physiology*, 117:500–544.

Hutter, O. F. and Noble, D. (1960). Rectifying properties of heart muscle. *Nature*, 188:495.

Inoue, R., Jensen, L. J. r., Shi, J., Morita, H., Nishida, M., Honda, A., and Ito, Y. (2006). Transient receptor potential channels in cardiovascular function and disease. *Circulation Research*, 99(2):119–31.

John, R. M., Tedrow, U. B., Koplan, B. A., Albert, C. M., Epstein, L. M., Sweeney, M. O., Miller, A. L., Michaud, G. F., and Stevenson, W. G. (2012). Ventricular arrhythmias and sudden cardiac death. *Lancet*, 380(9852):1520–9.

Jost, N., Virág, L., Bitay, M., Takács, J., Lengyel, C., Biliczki, P., Nagy, Z., Bogáts, G., Lathrop, D. a., Papp, J. G., and Varró, A. (2005). Restricting excessive cardiac action potential and QT prolongation: a vital role for IKs in human ventricular muscle. *Circulation*, 112(10):1392–9.

Jung, B.-C., Lee, S.-H., Cho, Y.-K., Park, H.-S., Kim, Y.-N., Lee, Y.-S., and Shin, D.-G. (2011). Role of the alternans of action potential duration and aconitine-induced arrhythmias in isolated rabbit hearts. *Journal of Korean Medical Science*, 26(12):1576–81.

Jurkat-Rott, K. and Lehmann-Horn, F. (2005). Muscle channelopathies and critical points in functional and genetic studies. *The Journal of Clinical Investigation*, 115(8):2000–9.

Kannankeril, P., Roden, D. M., and Darbar, D. (2010). Drug-induced long QT syndrome. *Pharmacological reviews*, 62(4):760–81.

Kherlopian, A. R., Ortega, F. A., and Christini, D. J. (2011). Cardiac myocyte model parameter sensitivity analysis and model transformation using a genetic algorithm. In *Proceedings of the 13th annual conference companion on Genetic and evolutionary computation - GECCO '11*, page 755, New York, New York, USA. ACM Press.

Kirchhof, P., Degen, H., Franz, M. R., Eckardt, L., Fabritz, L., Milberg, P., Läer, S., Neumann, J., Breithardt, G., and Haverkamp, W. (2003). Amiodarone-induced postrepolarization refractoriness suppresses induction of ventricular fibrillation. *Journal of Pharmacology and Experimental Therapeutics*, 305(1):257–263.

Krause, H., Antoni, H., and Fleckenstein, A. (1966). [An electronic model for the formation of local and transmitted stimuli on the myocardium fibers based upon variable current-voltage characteristics for potassium and sodium ions]. *Pflügers Archiv für die gesamte Physiologie des Menschen und der Tiere*, 289(1):12–36.

Kurz, R. W., Mohabir, R., Ren, X. L., and Franz, M. R. (1993). Ischaemia induced alternans of action potential duration in the intact-heart: dependence on coronary flow, preload and cycle length. *European Heart Journal*, 14(10):1410–20.

Lengyel, C., Iost, N., Virág, L., Varró, A., Lathrop, D. A., and Papp, J. G. (2001). Pharmacological block of the slow component of the outward delayed rectifier current (I(Ks)) fails to lengthen rabbit ventricular muscle QT(c) and action potential duration. *British journal of pharmacology*, 132(1):101–10.

Li, G.-R., Yang, B., Feng, J., Bosch, R. F., Carrier, M., and Nattel, S. (1999). Transmembrane ICa contributes to rate-dependent changes of action potentials in human ventricular myocytes. *The American Journal of Physiology*, 276(1 Pt 2):H98–H106.

Luo, C.-H. and Rudy, Y. (1991). A Model of the Ventricular Cardiac Action Potential: Depolarization, Repolarization and Their Interaction. *Circulation Research*, 68:1501–1526.

Luo, C.-H. and Rudy, Y. (1994a). A dynamic model of the cardiac ventricular action potential. I. Simulations of ionic currents and concentration changes. *Circulation Research*, 74(6):1071–96.

Luo, C.-H. and Rudy, Y. (1994b). A dynamic model of the cardiac ventricular action potential. II. Afterdepolarizations, triggered activity, and potentiation. *Circulation Research*, 74(6):1097–113.

Mahajan, A., Shiferaw, Y., Sato, D., Baher, A., Olcese, R., Xie, L.-H., Yang, M.-J., Chen, P.-S., Restrepo, J. G., Karma, A., Garfinkel, A., Qu, Z., and Weiss, J. N. (2008). A rabbit ventricular action potential model replicating cardiac dynamics at rapid heart rates. *Biophysical Journal*, 94(2):392–410.

Marder, E. and Taylor, A. L. (2011). Multiple models to capture the variability in biological neurons and networks. *Nature Neuroscience*, 14(2):133–8.

McAllister, R. E., Noble, D., and Tsien, R. W. (1975). Reconstruction of the electrical activity of cardiac Purkinje fibres. *The Journal of Physiology*, 251(1):1–59.

McIntosh, M. A., Cobbe, S. M., and Smith, G. L. (2000). Heterogeneous changes in action potential and intracellular Ca2+ in left ventricular myocyte sub-types from rabbits with heart failure. *Cardiovascular Research*, 45(2):397–409.

Nattel, S., Frelin, Y., Gaborit, N., Louault, C., and Demolombe, S. (2010). Ion-channel mRNA-expression profiling: Insights into cardiac remodeling and arrhythmic substrates. *Journal of molecular and cellular cardiology*, 48(1):96–105.

Niederer, S. A., Fink, M., Noble, D., and Smith, N. P. (2009). A meta-analysis of cardiac electrophysiology computational models. *Experimental Physiology*, 94(5):486–95.

Noble, D. (1960). Cardiac Action and Pacemaker Potentials based on the Hodgkin-Huxley Equations. *Nature*, 4749:495–497.

Noble, D. (1962). A modification of the Hodgkin-Huxley equations applicable to Purkinje fibre action and pace-maker potentials. *The Journal of Physiology*, 160:317–52.

Noble, D. (2011). Successes and failures in modeling heart cell electrophysiology. *Heart Rhythm : the Official Journal of the Heart Rhythm Society*, 8(11):1798–803.

Noble, D., Garny, A., and Noble, P. J. (2012). How the Hodgkin-Huxley equations inspired the Cardiac Physiome Project. *The Journal of Physiology*, 590(Pt 11):2613–28.

Noble, D. and Rudy, Y. (2001). Models of cardiac ventricular action potentials: iterative interaction between experiment and simulation. *Philosophical Transactions of the Royal Society A: Mathematical, Physical and Engineering Sciences*, 359(1783):1127–1142.

Nygren, A., Fiset, C., Firek, L., Clark, J. W., Lindblad, D. S., Clark, R. B., and Giles, W. R. (1998). Mathematical model of an adult human atrial cell: the role of K+ currents in repolarization. *Circulation research*, 82(1):63–81.

Prinz, A. A., Billimoria, C. P., and Marder, E. (2003). Alternative to hand-tuning conductance-based models: construction and analysis of databases of model neurons. *Journal of Neurophysiology*, 90(6):3998–4015.

Puglisi, J. L. and Bers, D. M. (2001). LabHEART: an interactive computer model of rabbit ventricular myocyte ion channels and Ca transport. *American Journal of Physiology. Cell Physiology*, 281(6):C2049–60.

Puglisi, J. L., Wang, F., and Bers, D. M. (2004). Modeling the isolated cardiac myocyte. *Progress in Biophysics and Molecular Biology*, 85(2-3):163–78.

Roden, D. M. (1998). Taking the "idio" out of "idiosyncratic": predicting torsades de pointes. *Pacing and Clinical Clectrophysiology : PACE*, 21(5):1029–34.

Roden, D. M., Balser, J. R., George, A. L., and Anderson, M. E. (2002). Cardiac ion channels. *Annual Review of Physiology*, 64:431–75.

Rodríguez, B., Trayanova, N. A., and Noble, D. (2006). Modeling cardiac ischemia. *Annals of the New York Academy of Sciences*, 1080:395–414.

Romero, L., Carbonell, B., Trénor, B., Rodríguez, B., Saiz, J., and Ferrero, J. M. (2010). Human and rabbit inter-species comparison of ionic mechanisms of arrhythmic risk: A simulation study. *Conference Proceedings : Annual International Conference of the IEEE Engineering in Medicine and Biology Society. IEEE Engineering in Medicine and Biology Society. Conference*, 2010:3253–6.

Romero, L., Carbonell, B., Trénor, B., Rodríguez, B., Saiz, J., and Ferrero, J. M. (2011). Systematic characterization of the ionic basis of rabbit cellular electrophysiology using two ventricular models. *Progress in Biophysics and Molecular Biology*, 107(1):60–73.

Romero, L., Pueyo, E., Fink, M., and Rodríguez, B. (2009). Impact of ionic current variability on human ventricular cellular electrophysiology. *American Journal of Physiology. Heart and Circulatory Physiology*, 297(4):H1436–45.

Rudy, Y. and Silva, J. R. (2006). Computational biology in the study of cardiac ion channels and cell electrophysiology. *Quarterly Reviews of Biophysics*, 39(1):57–116.

Sanguinetti, M. C. and Jurkiewicz, N. K. (1990). Two components of cardiac delayed rectifier K+ current. Differential sensitivity to block by class III antiarrhythmic agents. *The Journal of General Physiology*, 96(1):195–215.

Sanguinetti, M. C. and Jurkiewicz, N. K. (1992). Role of external Ca2+ and K+ in gating of cardiac delayed rectifier K+ currents. *Pflügers Archiv : European journal of physiology*, 420(2):180–6.

Sarkar, A. X., Christini, D. J., and Sobie, E. A. (2012). Exploiting mathematical models to illuminate electrophysiological variability between individuals. *The Journal of Physiology*, (212):2555–2567.

Sarkar, A. X. and Sobie, E. A. (2010). Regression analysis for constraining free parameters in electrophysiological models of cardiac cells. *PLoS Computational Biology*, 6(9):e1000914.

Sarkar, A. X. and Sobie, E. A. (2011). Quantification of repolarization reserve to understand interpatient variability in the response to proarrhythmic drugs: a computational analysis. *Heart Rhythm : the Official Journal of the Heart Rhythm Society*, 8(11):1749–55.

Schulz, D. J., Goaillard, J.-M., and Marder, E. (2006). Variable channel expression in identified single and electrically coupled neurons in different animals. *Nature Neuroscience*, 9(3):356–62.

Shannon, T. R., Wang, F., Puglisi, J. L., Weber, C., and Bers, D. M. (2004). A mathematical treatment of integrated Ca dynamics within the ventricular myocyte. *Biophysical Journal*, 87(5):3351–71.

Shaw, R. M. and Rudy, Y. (1997a). Electrophysiologic effects of acute myocardial ischemia. A mechanistic investigation of action potential conduction and conduction failure. *Circulation Research*, 80(1):124–38.

Shaw, R. M. and Rudy, Y. (1997b). Electrophysiologic effects of acute myocardial ischemia: a theoretical study of altered cell excitability and action potential duration. *Cardiovascular Research*, 35(2):256–72.

Shaw, R. M. and Rudy, Y. (1997c). Ionic mechanisms of propagation in cardiac tissue. Roles of the sodium and L-type calcium currents during reduced excitability and decreased gap junction coupling. *Circulation research*, 81(5):727–41.

Silva, J. and Rudy, Y. (2005). Subunit interaction determines IKs participation in cardiac repolarization and repolarization reserve. *Circulation*, 112(10):1384–91.

Sims, C., Reisenweber, S., Viswanathan, P. C., Choi, B.-R., Walker, W. H., and Salama, G. (2008). Sex, age, and regional differences in L-type calcium current are important determinants of arrhythmia phenotype in rabbit hearts with drug-induced long QT type 2. *Circulation Research*, 102(9):e86–100.

Sobie, E. A. (2009). Parameter sensitivity analysis in electrophysiological models using multivariable regression. *Biophysical Journal*, 96(4):1264–74.

Sobie, E. a. and Ramay, H. R. (2009). Excitation-contraction coupling gain in ventricular myocytes: insights from a parsimonious model. *The Journal of physiology*, 587(Pt 6):1293–9.

Spector, P. S., Curran, M. E., Zou, A., Keating, M. T., and Sanguinetti, M. C. (1996). Fast inactivation causes rectification of the IKr channel. *The Journal of general physiology*, 107(5):611–9.

Syed, Z., Vigmond, E., Nattel, S., and Leon, L. J. (2005). Atrial cell action potential parameter fitting using genetic algorithms. *Medical & biological engineering & computing*, 43(5):561–71.

Szentandrássy, N., Banyasz, T., Biro, T., Szabo, G., Toth, B. I., Magyar, J., Lazar, J., Varró, A., Kovacs, L., and Nanasi, P. P. (2005). Apico-basal inhomogeneity in distribution of ion channels in canine and human ventricular myocardium. *Cardiovascular Research*, 65(4):851–60.

Szigligeti, P., Pankucsi, C., Bányász, T., Varró, A., and Nánási, P. P. (1996). Action potential duration and force-frequency relationship in isolated rabbit, guinea pig and rat cardiac muscle. *Journal of Comparative Physiology. B, Biochemical, Systemic, and Environmental Physiology*, 166(2):150–5.

Taylor, A. L., Goaillard, J.-M., and Marder, E. (2009). How multiple conductances determine electrophysiological properties in a multicompartment model. *The Journal of Neuroscience*, 29(17):5573–86.

Taylor, J. A. and Lipsitz, L. A. (1997). Heart rate variability standards. *Circulation*, 95(1):280–1.

Terkildsen, J. R., Niederer, S., Crampin, E. J., Hunter, P., and Smith, N. P. (2008). Using Physiome standards to couple cellular functions for rat cardiac excitation-contraction. *Experimental physiology*, 93(7):919–29.

Vandenberg, J. I., Walker, B. D., and Campbell, T. J. (2001). HERG K+ channels: friend and foe. *Trends in pharmacological sciences*, 22(5):240–6.

Varró, A. and Baczkó, I. (2011). Cardiac ventricular repolarization reserve: a principle for understanding drug-related proarrhythmic risk. *British journal of pharmacology*, 164(1):14–36.

Varró, A., Baláti, B., Iost, N., Takács, J., Virág, L., Lathrop, D. A., Csaba, L., Tálosi, L., and Papp, J. G. (2000). The role of the delayed rectifier component IKs in dog ventricular muscle and Purkinje fibre repolarization. *The Journal of Physiology*, 523 Pt 1(2000):67–81.

Verkerk, A. O., Wilders, R., Veldkamp, M. W., de Geringel, W., Kirkels, J. H., and Tan, H. L. (2005). Gender disparities in cardiac cellular electrophysiology and arrhythmia susceptibility in human failing ventricular myocytes. *International Heart Journal*, 46(6):1105–18.

Virág, L., Acsai, K., Hála, O., Zaza, A., Bitay, M., Bogáts, G., Papp, J. G., and Varró, A. (2009). Self-augmentation of the lengthening of repolarization is related to the shape of the cardiac action potential: implications for reverse rate dependency. *British journal of pharmacology*, 156(7):1076–84.

Viswanathan, P. C. and Rudy, Y. (1999). Pause induced early afterdepolarizations in the long QT syndrome: a simulation study. *Cardiovascular research*, 42(2):530–42.

Wagner, M. B., Namiki, T., Wilders, R., Joyner, R. W., Jongsma, H. J., Verheijck, E. E., Kumar, R., Golod, D. A., Goolsby, W. N., and van Ginneken, A. C. G. (1999). Electrical interactions among real cardiac cells and cell models in a linear strand. *American Journal of Physiology. Heart and Circulatory Physiology*, 276:H391–H400.

Walmsley, J., Mirams, G., Bahoshy, M., Bollensdorff, C., Rodríguez, B., and Burrage, K. (2010). Phenomenological modeling of cell-to-cell and beat-to-beat variability in isolated Guinea Pig ventricular myocytes. *Conference Proceedings : Annual International Conference of the IEEE Engineering in Medicine and Biology Society. IEEE Engineering in Medicine and Biology Society. Conference*, 2010:1457–60.

Walmsley, J., Rodriguez, J. F., Mirams, G., Burrage, K., Efimov, I., and Rodriguez, B. (2013). mRNA Expression Levels in Failing Human Hearts Predict Cellular Electrophysiological Remodeling : A Population-Based Simulation Study. *PloS One*.

Wu, L., Ma, J., Li, H., Wang, C., Grandi, E., Zhang, P., Luo, A., Bers, D. M., Shryock, J. C., and Belardinelli, L. (2011). Late sodium current contributes to the reverse rate-dependent effect of IKr inhibition on ventricular repolarization. *Circulation*, 123(16):1713–20.

Xiao, L., Xiao, J., Luo, X., Lin, H., Wang, Z., and Nattel, S. (2008). Feedback remodeling of cardiac potassium current expression: a novel potential mechanism for control of repolarization reserve. *Circulation*, 118(10):983–92.

Yan, G.-X., Rials, S. J., Wu, Y., Liu, T., Xu, X., Marinchak, R. A., and Kowey, P. R. (2001). Ventricular hypertrophy amplifies transmural repolarization dispersion and induces early afterdepolarization. *American Journal of Physiology. Heart and Circulatory Physiology*, 281:H1968–H1975.

Yang, T., Snyders, D. J., and Roden, D. M. (1997). Rapid inactivation determines the rectification and [K+]o dependence of the rapid component of the delayed rectifier K+ current in cardiac cells. *Circulation research*, 80(6):782–9.

Zabel, M., Hohnloser, S. H., Behrens, S., Woosley, R. L., and Franz, M. R. (1997a). Differential effects of D-sotalol, quinidine, and amiodarone on dispersion of ventricular repolarization in the isolated rabbit heart. *Journal of Cardiovascular Electrophysiology*, 8(11):1239–45.

Zabel, M., Woosley, R. L., and Franz, M. R. (1997b). Is dispersion of ventricular repolarization rate dependent? *Pacing and Clinical Electrophysiology : PACE*, 20(10 Pt 1):2405–11.

Zeng, J., Laurita, K. R., Rosenbaum, D. S., and Rudy, Y. (1995). Two Components of the Delayed Rectifier K+ Current in Ventricular Myocytes of the Guinea Pig Type : Theoretical Formulation and Their Role in Repolarization. *Circulation Research*, 77(1):140–152.